PAPER

Uptake and diffusion of plasma-generated reactive nitrogen species through keratinized membrane

To cite this article: Yeon-Ho Im *et al* 2019 *J. Phys. D: Appl. Phys.* **52** 195201

IOP Publishing Journal of Physics D: Applied Physics
J. Phys. D: Appl. Phys. **52** (2019) 195201 (11pp) https://doi.org/10.1088/1361-6463/ab0867

Uptake and diffusion of plasma-generated reactive nitrogen species through keratinized membrane

Yeon-Ho Im[1], Zilan Xiong[2], Daniel T Elg[3] and David B Graves[4,5]

[1] Department of Chemical Engineering, Chonbuk National University, Jeonju, Republic of Korea
[2] State Key Laboratory of Advanced Electromagnetic Engineering and Technology, Huazhong University of Science and Technology, Wuhan, People's Republic of China
[3] Department of Engineering, University of Southern Indiana, Evansville, IN, United States of America
[4] Department of Chemical and Biomolecular Engineering, University of California, Berkeley, Berkeley, CA, United States of America

E-mail: graves@berkeley.edu (D Graves)

Received 3 December 2018, revised 9 February 2019
Accepted for publication 19 February 2019
Published 5 March 2019

Abstract

We propose a mathematical model for uptake and diffusion of air plasma-generated reactive nitrogen species (RNS) in a model keratinized membrane, such as a thin slice of bovine hoof or human nail material. An experimental system consisting of a surface microdischarge (SMD) in air was designed for the purpose of developing and validating a reaction-diffusion model to describe this system. Key variables such as membrane effective diffusivity, surface reaction rate coefficients, and other parameters are determined through comparison between the model predictions and experimental measurements. The model results yield spatial and temporal concentration profiles of RNS inside the keratinized membrane, leading to an improved understanding of transport and reaction of plasma generated RNS through the membrane. This work offers insights into possible mechanisms underlying plasma treatment of toenail fungus.

Keywords: atmospheric pressure plasma, plasma medicine, RONS, plasma–liquid interactions, antifungal, onychomycosis, plasma modeling

(Some figures may appear in colour only in the online journal)

1. Introduction

Cold atmospheric-pressure air plasmas (CAP) have been studied for a wide range of applications in plasma medicine, in part due to the generation of reactive oxygen and nitrogen species (RONS) at ambient or near-ambient conditions [1–6]. It has been demonstrated that atmospheric-pressure, ambient temperature gas plasmas are promising platforms for a wide range of environmental and biomedical applications based on their demonstrated antimicrobial action, treatment of infected tissue, and disinfection of wounds, among many others [1, 7–10]. However, plasma technologies face challenges in many applications because of the intrinsically complex nature of plasma interactions with biomaterials coupled with complex and not fully characterized plasma-biomaterial effects [7]. There is little doubt that the current lack of basic understanding of plasma interactions with biomaterials is a significant challenge that must be overcome in order to more widely enable applications of plasma medicine.

As a part of the ongoing set of efforts to address these emerging issues, this work focuses on modeling diffusive transport of reactive nitrogen species (RNS) with heterogeneous reactions inside a model porous biomaterial. The model is designed to approximate a physical experimental setup detailed previously [11, 12], in which a plasma source was used to inactivate either *T. rubrum* or *Escherichia coli* K12 on the far side of a slice of bovine hoof. *T. rubrum* is a common human toenail fungus responsible for onychomycosis and *E. coli* serves as a convenient model microbial target. The bovine hoof slice is a keratin membrane that also serves as

[5] Author to whom any correspondence should be addressed.

a model for human nail [13, 14]. In this work, uptake and delivery of RNS inside the model keratin bio-membrane were analyzed using a transient reaction-diffusion model. In the present model, we postulate that the major active RNS created by the plasma is NO_2, and that this NO_2 diffuses through the porous keratin to reach microbes residing on the back side of the membrane. When compared with experiments, the reaction-diffusion model shows evidence that RNS cause an antimicrobial effect by penetrating through the porous keratin membrane. Additionally, it is shown that adsorbed H_2O on the membrane surface initially causes hydrolysis of plasma-produced NO_2, creating HNO_3 and preventing NO_2 from reaching the far side of the nail. Once the active sites for hydrolysis have been consumed, NO_2 can diffuse through the nail and reach the other side. The rate of bacterial inactivation on the back side of the membrane correlated reasonably well with measured rates of NO_2 penetration through the nail, lending support to the original hypothesis. These results offer insights into the likely mechanism of plasma treatment of onychomycosis and possibly for other plasma-biomaterial treatments as well.

2. Setup

2.1. Experimental

The experimental setup used for comparison to the model is similar to one detailed previously [11]. As shown in inset of figure 1, a surface micro-discharge (SMD) device was used to generate RNS under the higher-power nitrogen oxides-dominated mode [12]. The SMD device configuration, gas-phase spectroscopy, analysis of aqueous chemistry, and antifungal experiments were described in detail in our previous report [12, 15]. Briefly, the SMD, operating in an enclosed acrylic chamber in atmospheric air, was powered with a 2.5 kV sinusoid at a frequency of 25 kHz. As shown in figure 1, the SMD was attached to the top of a chamber set up as a Franz cell, with the top cell and bottom cell separated by a slice of bovine hoof. The seal between the hoof material and the acrylic surfaces of the container was tested to minimize any transport between the membrane and the acrylic. The gas-phase plasma-generated species were quantified above the hoof slice by Fourier transform infrared absorption spectroscopy (FTIR). Penetration of the hoof slice by RNS was measured using Griess reagent (via UV/VIS absorption spectrometry detecting aqueous NO_2^-) in phosphate buffered saline (PBS) placed in the bottom cell. For antibacterial experiments, *Escherichia coli* K12 was cultured and prepared as described in previous work [11]. To seed the hoof with bacteria, hoof slices were washed with sterile water and dried until lack of visible hydration before being pelleted with *E. coli* prior to plasma exposure.

Although not shown here, the effective diffusivity (D_{eff}) in the hoof disk, in the absence of reaction, was measured directly using an experimental setup similar to the one depicted in figure 1, employing CH_4 and CO_2. The estimated D_{eff} in this work was 5.0×10^{-5} cm^2 s^{-1}, which is similar to diffusion coefficients of other small molecules diffusing through living tissue [16–19].

2.2. Model

Transport of plasma-produced NO_2 through the hoof membrane was modeled by a transient, 1D reaction-diffusion equation within the hoof slice:

$$\varepsilon \frac{\partial C_{\text{NO}_2,\text{hoof}}}{\partial t} = D_{\text{eff}} \frac{\partial^2 C_{\text{NO}_2,\text{hoof}}}{\partial x^2} - R_{\text{hoof}} \tag{1}$$

where ε, $C_{\text{NO}_2,\text{hoof}}$, D_{eff}, and R_{hoof} represent the porosity of hoof disk, the concentration of NO_2, the effective diffusivity of NO_2 within the hoof membrane, and the net rate of chemical reactions with NO_2 inside the hoof membrane, respectively. In this work, the porosity of hoof disk was taken as 0.05, based on cumulative mercury intrusion data into bovine hoof reported in the literature [14]. The measured gas phase NO_2 concentration, shown in figure 1, was used directly as a time-dependent boundary condition at the interface between the plasma and the top of the hoof membrane.

NO_2-consuming reactions inside the porous hoof membrane can in principle occur in both the gas phase and on the surface of the membrane material. While NO_2 is fairly stable in the gas phase on the timescales considered here, it is known to undergo reversible dimerization to N_2O_4, as shown in reaction (R1),

$$2NO_2 \overset{k_1,\, k_{-1}}{\longleftrightarrow} N_2O_4. \tag{R1}$$

For the concentrations of NO_2 measured in figure 1 and the values of the relevant forward and reverse rate constants ($K_{1,\text{gas}} = k_1/k_{-1} = 6.86$ atm^{-1}) [20], the calculated dimer concentration is approximately two orders of magnitude below that of NO_2, as shown in figure 1. Due to the rate constants and the presence of a dense, porous membrane, Knudsen diffusion was assumed within the hoof membrane, allowing for gas-phase dimerization within the hoof volume to be ignored. Thus, only NO_2 was considered in equation (1) for diffuse transport and surface reaction.

When considering reactions with the internal surface of the porous hoof membrane, it is important to note that keratin is generally coated with a layer of water adsorbed from the atmosphere, which is likely to dominate NO_2-hoof material interactions. Thus, it is important to understand the nature of this adsorbed water. Detailed water uptake isotherms have been reported for keratin tissues such as human nail, horn, hair and wool [21]. It was shown that the water uptake behavior on keratin follows a Langmuir isotherm at lower humidity because water molecules are bonded to hydrophilic surface sites. Therefore, it is clear that the monolayer of adsorbed water is not the equivalent of bulk water. The adsorption of a monolayer of water in a keratin structure has been reported as 0.06 g H_2O/g dry keratin [21]; that number is used in this work as the water uptake in the hoof membrane.

There has, as yet, been no report in the literature regarding the detailed mechanism of NO_2 uptake by keratin-based material. However, it has been reported that the heterogeneous hydrolysis reaction of NO_2 on carbonaceous particles and protein dust is the main mechanism to explain NO_2 uptake in the presence of humidity. Furthermore, there appears to be

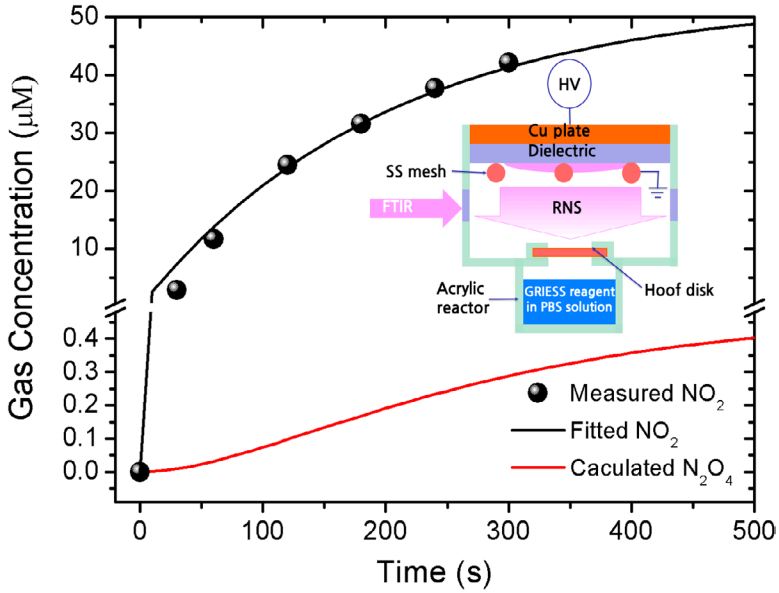

Figure 1. NO_2 gas concentration as a function of time measured by gas-phase FTIR absorption spectroscopy. The data points are numerically fitted to provide an input of NO_2 for the reaction-diffusion model boundary condition at the top of the hoof disk. The gas phase concentration of N_2O_4, calculated based on equilibrium data, is insignificantly small under these conditions. The inset represents a schematic diagram of the experiment.

relatively low direct reactivity of NO_2 with protein-containing materials in the absence of humidity [22–27]. Because of high water uptake of keratin-based materials, it is reasonable to assume that the hydrolysis reaction of NO_2 with absorbed water on the surface of membrane fibers would lead to NO_2 uptake on the hoof disk interior surfaces. As described in a later section, it should be noted that our experimental evidence of NO_2 penetration supports the plausibility of this assumption.

In part, the proposed uptake model is based on similar research from the [28–31]. NO_2 uptake in the presence of water on mineral dust or soot particles suspended in the atmosphere is an important process in models of atmospheric chemistry. The uptake model we chose is based on kinetic theory, assuming an ideal gas and an Eley–Rideal mechanism, in which the rate-limiting step is assumed to be the adsorption of NO_2 as shown in reaction (R2) [28, 32, 33]:

$$2NO_2\,(g) + H_2O\,(s) \rightarrow N_2O_4 \cdot H_2O\,(s) \qquad \text{(R2)}$$

$$N_2O_4 \cdot H_2O\,(s) \rightarrow HNO_2\,(g, s) + HNO_3(s). \qquad \text{(R3)}$$

Since reaction (R2) is a surface reaction, a surface site balance equation is written for adsorbed water reacting with gas phase NO_2, in the following form:

$$\frac{d\theta_{H_2O}}{dt} = -\gamma_{NO_2}\theta_{H_2O}J_{NO_2}\sigma_{H_2O}. \qquad (2)$$

Here, θ_{H_2O} denotes the fractional surface coverage of H_2O that has not yet reacted with NO_2; thus, as more H_2O reacts with NO_2, the coverage of H_2O still available for NO_2 uptake reactions decreases. In the present model, we assume that NO_2, after adsorbing on the surface water layer, is inactive and the resulting water-NO_2 surface compound will not adsorb any additional water. The uptake coefficient of NO_2 on water absorbed in keratin material, γ_{NO_2}, has been intensively researched to develop realistic atmospheric chemistry models, but values reported in the literature range from ~10^{-4} to ~10^{-6} based on whether the coefficient was measured for droplets, aerosols, or thin films [28, 34, 35]. The thin film uptake coefficient of 10^{-6} will be used in this paper as it seems to be most appropriate for porous keratin. The effective molecular cross section of water on the surface, σ_{H_2O}, is assumed to be 0.124 nm^2. The surface collision frequency per unit area, J_{NO_2}, can be expressed as the average gas kinetic flux in equation (3),

$$J_{NO_2} = C_{NO_2,hoof}\omega_{NO_2}/4 \qquad (3)$$

where ω_{NO_2} is thermal velocity of NO_2, given by equation (4):

$$\omega_{NO_2} = \sqrt{\frac{8RT}{\pi m_{NO_2}}}. \qquad (4)$$

Here, m_{NO_2} is the molar mass of NO_2, R is the gas constant, and T is the absolute temperature.

Finally, it is necessary to write an equation for the total uptake of NO_2 by water on the surface of the hoof membrane fibers, which will correspond to R_{hoof}, the total loss of NO_2 from reactions inside the hoof volume in equation (1). This uptake will be proportional to the total number of available water sites per unit volume of hoof material, the flux of NO_2, and the NO_2 uptake coefficient. The total number of available sites for NO_2 reaction can be written as:

$$\#\text{available sites} = \frac{\rho_{hoof}}{M_w}\, v_{m_{reactive}}\sigma_{H_2O}\theta_{H_2O} \qquad (5)$$

where ρ_{hoof} is the mass density of the hoof membrane, M_w is the molar mass of H_2O, and $v_{m_{reactive}}$ is the amount of water that actually takes part in hydrolysis of NO_2. The dry density of bovine hoof is regarded as 1.3 g cm^{-3} of human nail with the similar keratin structure due to absence of proper experimental

data [36]. Not all adsorbed water takes part in hydrolysis, and $v_{m_{\text{reactive}}}$ is calculated as

$$v_{m_{\text{reactive}}} = \phi v_m \tag{6}$$

where ϕ is an adjustable constant determined by comparison to experiments. The determination of this constant will be discussed in the next section. Multiplying equation (5) by the flux of NO_2 and the NO_2 uptake coefficient yields equation (7) for R_{hoof}:

$$R_{\text{hoof}} = \frac{\gamma_{NO_2}\theta_{H_2O}J_{NO_2}\rho_{\text{hoof}}v_{\text{m\_reactive}}\sigma_{H_2O}}{M_w}. \tag{7}$$

Thus, if equation (7) is inserted into equations (1) and (3) is plugged into equation (2), equations (1) and (2) become a coupled set of differential equations that can be solved for the concentration of NO_2 and the fractional coverage of available surface sites.

Once NO_2 penetrates through the entire hoof membrane, it then diffuses through a small air gap of 5 mm and into a reservoir of PBS solution containing Griess reagent (see figure 1). In modeling this transport and water solvation, we followed the approach reported by Deen's group. In this approach, the differential equations and computational complexity were simplified by defining a 'total reactive nitrogen' concentration [20];

$$C_N = C_{NO_2} + 2C_{N_2O_4}. \tag{8}$$

According to this approach, it is assumed that NO_2 and N_2O_4 are near equilibrium in the liquid or gas. Thus, solving coupled diffusion-reaction equations for each species is unnecessary, and based on reaction (R1), the concentrations of N_2O_4 in air and water can be written as

$$C_{N_2O_4,\text{air}} = K_{1,\text{air}}\text{RT}C^2_{NO_2,\text{air}} \tag{9}$$

$$C_{N_2O_4,\text{water}} = K_{1,\text{water}}C^2_{NO_2,\text{water}} \tag{10}$$

where $K_{1,\text{water}}$ represents the dimerization equilibrium constant of NO_2 in the liquid phase and is assumed to be 6.54×10^4 M^{-1} [20, 33]. Assuming that the gas-phase and liquid-phase diffusivities (D_{air} and D_{water}) of NO_2 and N_2O_4 are equal, the transient diffusion-reaction equation for each phase can be written as:

$$\frac{\partial C_{N,I}}{\partial t} = D_{N,I}\frac{\partial^2 C_{N,I}}{\partial x^2} + R_I \tag{11}$$

where I denotes either air or water. Here, $D_{N,\text{air}}$ and $D_{N,\text{liquid}}$ are taken as 1.7×10^{-5}, and 1.85×10^{-9} m^2 s^{-1}, respectively [35]. At the interface between air and water, the liquid-phase concentration is governed by Henry's Law:

$$C_{N,\text{water,interfacial}} = \text{RT}\left(h_{NO_2}C_{NO_2,\text{gas,interfacial}} + h_{N_2O_4}C_{N_2O_4,\text{gas,interfacial}}\right). \tag{12}$$

Henry's law coefficients h_{NO_2} and $h_{N_2O_4}$ are 9×10^{-3} and 0.77 M atm^{-1}, respectively [20, 37].

Due to the 'total reactive nitrogen' assumption in equations (8)–(10), the loss due to reactions in the gas phase in equation (11) is set to 0. In buffered liquid solutions containing Griess reagent, we considered the following hydrolysis reaction of N_2O_4 which is in equilibrium with NO_2, as justified elsewhere [20].

$$N_2O_4 + H_2O \xrightarrow{k_2} HNO_2 + HNO_3. \tag{R4}$$

The uptake and hydrolysis of gas phase NO_2 in liquid water play important roles in various fundamental atmospheric and environmental chemistries [20, 22, 30]. Due to the apparent absence of real-time monitoring of these species under hydrolysis conditions, most analyses rely on theoretical estimates in order to determine chemical mechanisms and rates [22, 38–40]. Recently, Deen's group reported that the accumulation rates of NO_2^- and NO_3^- in buffered aqueous solutions with exposure to NO_2 gas follow the stoichiometry of reaction (R4) [20]. Their reported experimental measurements were consistent with these assumptions. We have therefore followed their approach in the present work.

The loss due to reactions in the liquid phase is given by equation (13):

$$R_{\text{liquid}} = -k_2 C_{N_2O_4} \tag{13}$$

where k_2 is the reaction rate coefficient in reaction (R4) (assumed to be the same as in reaction (R3)), given as 10^3 s^{-1} [20]. The detailed boundary conditions expressions using total reactive nitrogen concentration are found in [20]. Note that the model prediction of formation of HNO_2 in (R4) is assumed to lead to the formation of nitrite (NO_2^-), the compound detected experimentally using Greiss reagent.

The 1D transient reaction-diffusion equation for transport and reaction in the porous membrane (equation (1)) and for subsequent diffusion and water dissolution (equation (11)) are coupled with equation (2) for water surface coverage at each point within the porous membrane as a function of time. There, equations were numerically solved using Mathematica.

3. Results and discussion

In this model, all variables except the proportionality constant (ϕ) can be independently estimated using published data. Adjusting ϕ effectively alters the extent to which NO_2 uptake occurs within the membrane. Setting this parameter to zero eliminates uptake, resulting in pure diffusion of NO_2 through the membrane with no loss at the porous nail surface. Physically, this key parameter corresponds to the fraction of water that participates in uptake. Water uptake inside the keratin fibers can be reduced during NO_2 uptake because the surface reactions of (R2) and (R3) in the liquid phase are exothermic reactions with reaction enthalpy of −63.38 KJ mol^{-1}. In addition to that, it is desirable that we also consider the existence of both 'bound' and 'free' water on the keratin fibers, where 'bound' water is not available to take part in reactions. To the best of the authors' knowledge, the details regarding the above phenomena have not been reported in the literature so far, and rates for these processes are difficult to theoretically estimate. Therefore, the inclusion of this parameter in this work is to simplify the complexities of NO_2 uptake.

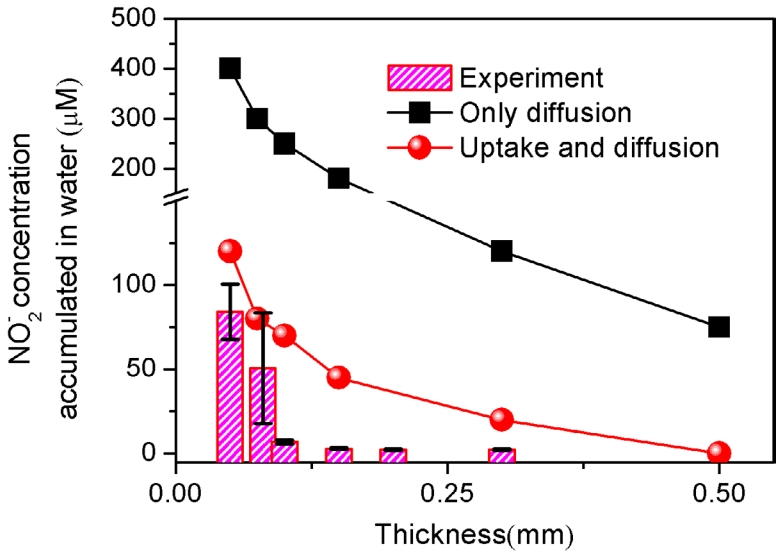

Figure 2. Penetration of the hoof membrane by NO_2 as a function of hoof thickness, as measured by nitrite ion concentration accumulated in the water reservoir beneath the hoof membrane after 20 min exposure. If only diffusion is considered in the model, far more penetration of NO_2 is predicted than what is experimentally observed. If NO_2 uptake by surface hydrolysis in adsorbed water is included with a proportionality constant of $\varphi = 10^{-3}$, reasonable agreement is found between the model and experiment (see text). This suggests that approximately 0.1% of the adsorbed water takes part in NO_2 uptake by hydrolysis, inhibiting transport through the hoof membrane.

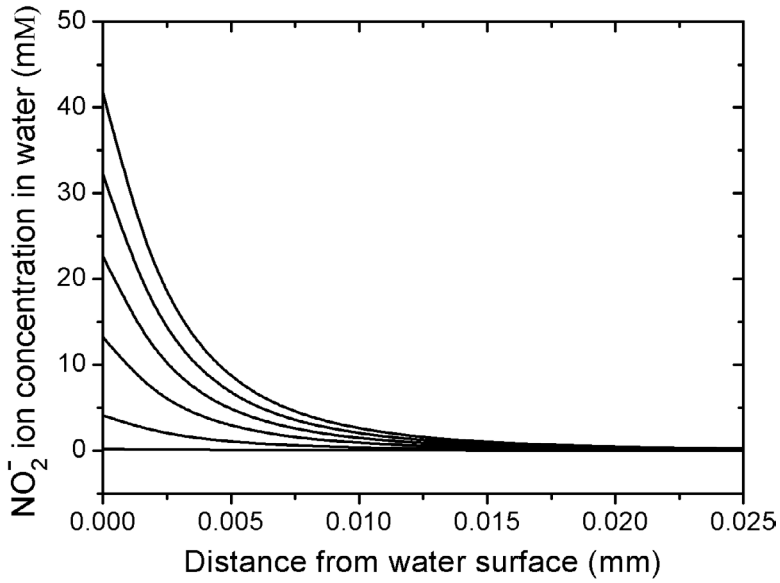

Figure 3. Modeling results of the time- and space-profiles of nitrite ion concentration diffusing into the water surface, shown in the lower region of the container in figure 1. Each profile represents a 4 min increment, starting at 0 min. It should be noted that, for minutes 8–20, the concentration of nitrite at the water surface (0 mm) rises by the same amount every increment; this implies a linear rise of nitrite at the water surface as a function of time.

It was inferred in this work by comparison between model and measurements.

To address this issue, we used Griess reagent measurements to determine the accumulation of aqueous nitrite formed by the plasma-generated RNS inside the water reservoir after penetration of the hoof, as shown in figure 1. The hoof membrane thickness was varied, and multiple experiments were conducted with different membrane thicknesses. As shown in figure 2, the measured nitrite concentration in the water after 20 min exposure strongly depends on the thickness of the bovine hoof. This indicates clearly that the plasma-generated NO_2 can be transported by diffusion through the hoof membrane. However, if φ is set to 0 (corresponding to no surface loss of NO_2) and only diffusion through the porous nail is considered, the model results do not agree well with the experimental results. Thus, it is likely that diffusive transport through the membrane is hindered by uptake with surface-bound, reactive water. By including uptake in the model with a proportionality constant of $\varphi = 10^{-3}$, agreement between experiment and model is significantly improved. This result suggests that a small portion of adsorbed water takes part in uptake and hydrolysis of NO_2, indicating that most adsorbed water on the surface of the keratin is strongly bound and therefore does not inhibit diffusion of NO_2 through the membrane.

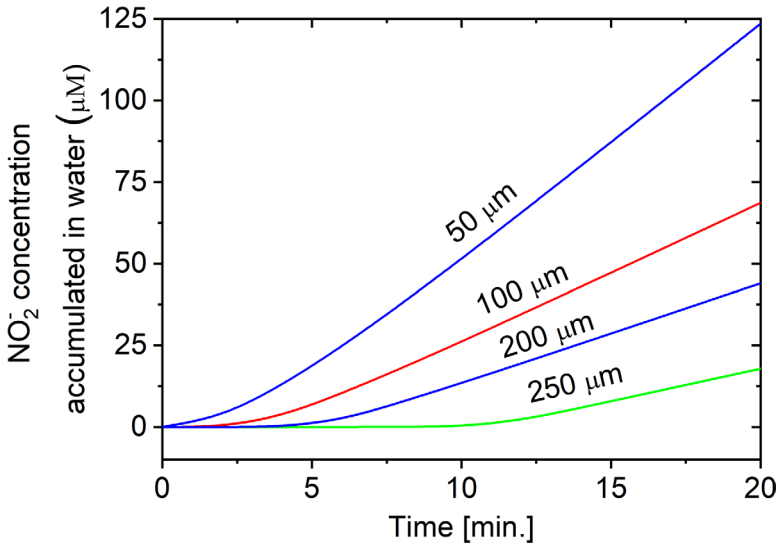

Figure 4. The average simulated nitrite concentration in the reservoir of water beneath the hoof is shown as a function of time for varying hoof thicknesses. This corresponds to penetration of the hoof membrane by NO_2. As expected, penetration decreases with increasing hoof thickness. Additionally, all hoof membranes appear to display an 'induction time' in which the nitrite concentration remains near 0, followed by a period in which the nitrite concentration increases linearly (corresponding to constant penetration). The induction time corresponds to NO_2 uptake by adsorbed water on the keratin fibers; only after uptake is complete can NO_2 penetrate the hoof membrane.

Having estimated the proportionality factor for free water in this manner, the parameter was held constant for the remainder of the simulations. The model was used to explore physical processes occurring in the penetration of NO_2 through the hoof membrane as well as accumulation of nitrite both within the nail material as well as in the reservoir of water (see figure 1) below the nail. Figure 3 shows predicted nitrite concentration spatial profiles near the surface of the pool of water (on the back side of the membrane) for a 250 μm-thick hoof (approximately the same thickness as a human nail) at time increments of 4 min.

As shown in figure 3, the concentration of nitrite at the surface of the water initially rises slowly. However, after the first 8 min, this concentration appears to rise linearly in time, increasing by approximately 9 mM every 4 min. This effect is further explored in figure 4. If the nitrite concentration profile is spatially averaged over the pool of water (to simulate mixing), the average nitrite concentration is shown to follow this type of behavior for a variety of hoof thicknesses.

Figure 4 shows nitrite accumulation profiles in the pool of water beneath the hoof (following hoof membrane penetration) as a function of time for various hoof thicknesses. Two important results can be observed. First, NO_2 penetration of the hoof decreases as the hoof thickness increases. Second, each hoof appears to have an 'induction time' in which the accumulated nitrite concentration in the water adjacent to the nail stays at 0. Accordingly, penetration of the hoof membrane by NO_2 is non-existent during this time. This 'induction time' corresponds to uptake and hydrolysis of NO_2 by adsorbed water within the hoof. Once uptake of NO_x into hoof is complete, corresponding to complete saturation of free surface sites, NO_2 can fully penetrate the hoof membrane and reach the underlying water. After this time, the nitrite concentration begins to increase, quickly reaching a point at which it accumulates linearly with time. At this point, the rate of penetration of NO_x through the hoof membrane reaches its steady-state value. Transport through the hoof after saturation occurs through pure diffusion, since the number of available surface sites has gone to zero. Increasing the hoof thickness not only decreases the nitrite accumulation rate (i.e. penetration of the nail occurs more slowly) but also lengthens the induction time (since a thicker membrane presents more surface sites for NO_2 uptake). Thus, in through-nail plasma treatment of onychomycosis, nail thickness will likely play a key role.

This interpretation can be directly verified by exploring phenomena within the hoof membrane. Figure 5 shows fractional coverage of the keratin fibers by available hydrolysis surface sites inside the 250 μm-thick at 2 min intervals. As time increases, NO_2 first depletes the available surface sites near the top of the hoof membrane, sending θ_{H_2O} to 0 at that location rather quickly. As uptake is completed near the top of the hoof, NO_2 progresses deeper into the hoof, depleting surface sites and causing θ_{H_2O} to drop to 0 farther below the surface of the hoof. After 8 min, θ_{H_2O} does not reach 100% at any location inside the membrane; by 12 min, it does not rise above 20% even at the far end of the hoof. This corresponds to the time in figure 4 at which NO_2 begins to significantly penetrate the hoof and accumulate as nitrite in the underlying water. Figure 6 displays the same phenomenon in terms of NO_2 gas phase concentration inside the hoof membrane. The propagation of NO_2 species inside the hoof is characterized by relatively slow diffusion through the pores of the membrane as well as by the uptake of NO_2 by water on the surface of the keratin. When compared to figure 5, it is clear that NO_2 penetration drops to 0 at the point where active surface sites have not yet been depleted. As NO_2 depletes active surface sites, it is able to penetrate deeper into the nail, eventually reaching the far side. The time- and position-dependent profile of NO_2 concentration within the membrane behaves as a propagating wave.

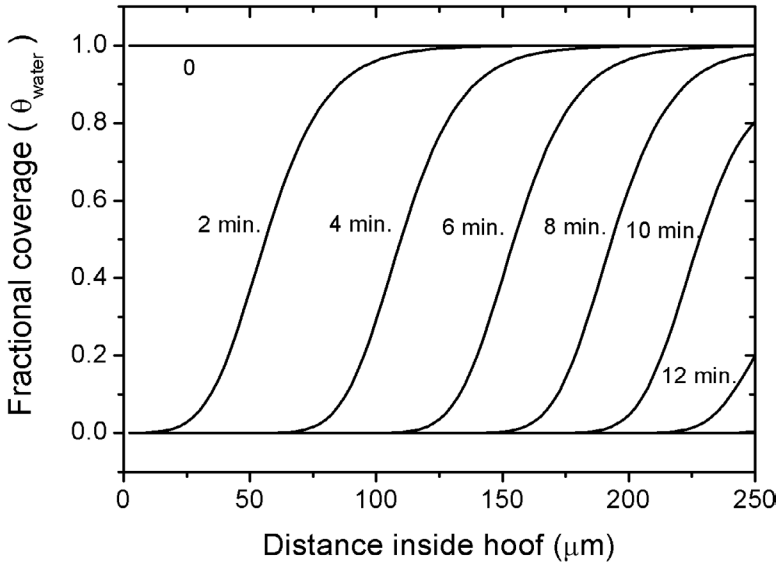

Figure 5. Plot of the time and position dependence of fractional surface water coverage within a 250 μm thick hoof slice. When NO_2 is incident on the membrane, it initially undergoes uptake and hydrolysis by adsorbed water, depleting active surface sites for uptake. Once surface sites at a certain depth are depleted, NO_2 can penetrate farther into the hoof, progressively depleting surface sites until all active sites are saturated. The nearly-complete elimination of active sites at 12 min corresponds to the end of the 'induction time' in figure 4 and the ability of NO_2 to penetrate through the entire hoof.

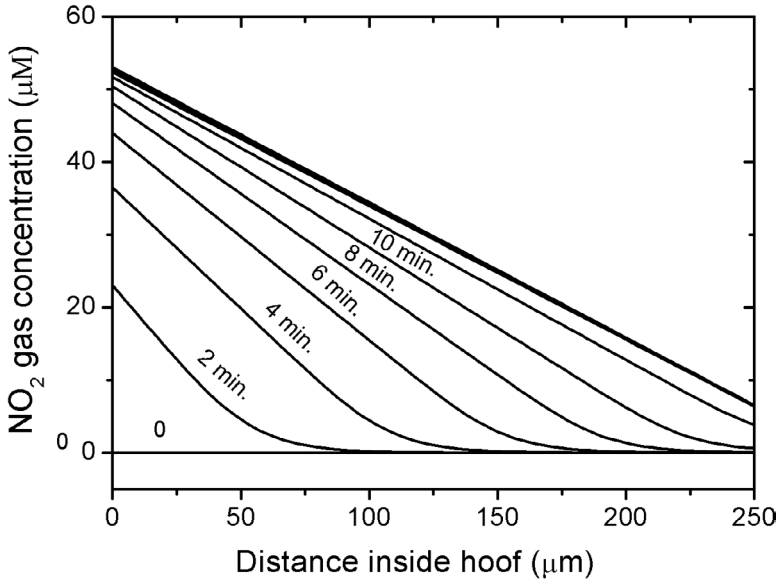

Figure 6. NO_2 concentration profiles at different times inside the hoof membrane, corresponding to figure 5. The penetration of NO_2 through the hoof corresponds approximately to the location at which the surface coverage rises from 0% to 100% in figure 5.

Finally, to understand the effect of these modeled mechanisms on through-nail plasma treatment, antibacterial activity was investigated experimentally and compared to simulations. Antibacterial activity was measured by means of log reductions after plasma treatments of varying time, in which the log reduction is given by

$$\text{log reduction} = \log\left(\frac{N_0}{N}\right) \tag{14}$$

where N_0 is the number of viable cells present in an untreated sample and N is the number of cells that remained viable treatment after plasma exposures. Detailed experimental procedures for the bacterial experiments were reported previously, as noted above [11, 12]. Experiments were undertaken with *E. coli* on both the top of the hoof membrane and the bottom of the hoof membrane with membrane thickness of 250 μm. Although the primary interest is in measuring the bacterial kill on the backside of the membrane, the top side measurements help establish the concentration-time relationship between NO_2 and bacterial inactivation rates and can be compared to previous results to assure consistency. Figure 7 shows a comparison of the measured averaged NO_2 gas concentration and bacteria log reduction as a function of time at the top of the hoof.

As shown in figure 7, bacterial inactivation at the top of the hoof initially correlates reasonably well with NO_2

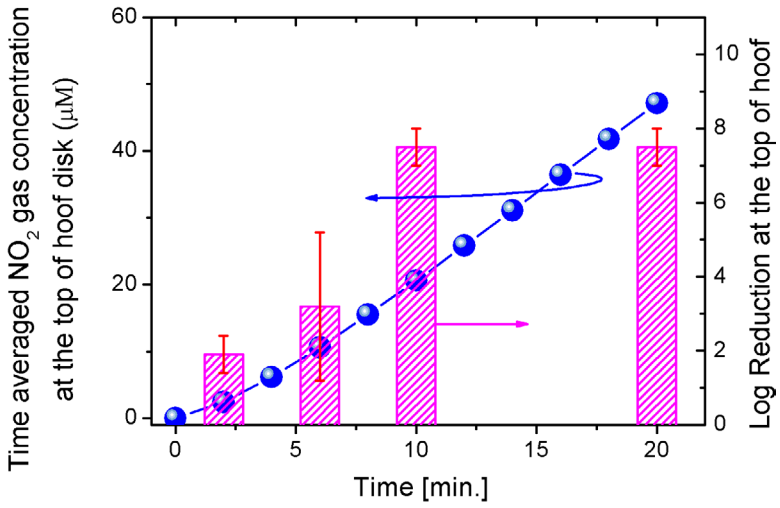

Figure 7. Antibacterial activity (vertical bars with error bars) is measured at the top (adjacent to SMD plasma side) of a hoof membrane as compared to measured NO_2 concentration (symbols) above the hoof. For treatments of less than 10 min, the NO_2 concentration correlates reasonably well with the log reduction; for 10 min and longer, the log reduction appears to saturate. NO_2 inactivated nearly all surface bacteria within 10 min.

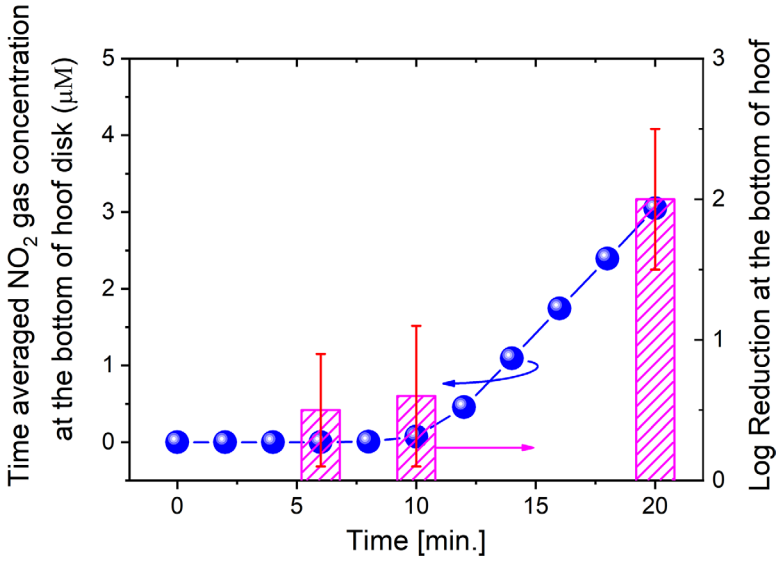

Figure 8. When *E. coli* is present on the far side of the 250 μm thick hoof membrane, log reduction correlates reasonably well with simulated NO_2 concentration on the backside. The inset shows predicted gas phase HNO_2 inside the nail (see text below). As previously shown, active uptake sites within the membrane must be depleted before NO_2 can penetrate to the other side in significant amounts. Accordingly, little bacterial killing is seen before the completion of uptake and hydrolysis. After 10 min, active surface sites are predicted to be completely depleted and the NO_2 concentration rises. Measured bacterial loss appears to correlate with model prediction of NO_2 breakthrough.

concentration and is consistent with previously reported data for similar experiments in killing *E. coli* using SMD air plasma [11, 12]. The bacterial log reduction appears to saturate after 10 min exposure, since the maximum log reduction possible, given the initial bacterial load, was about 8.

Figure 8 shows results for treatment of bacteria on the far side of the hoof membrane, which is more applicable to scenarios such as through-nail treatment of onychomycosis.

As shown in figure 8, the log reduction of bacteria on the bottom side of the hoof appears to correlate with predicted NO_2 concentration at this location. Since NO_2 concentrations are smaller than on the top of the hoof, the log reduction is not saturated even after 20 min exposure. Note that the 20 min NO_2 concentration at the bottom of the hoof is about the same as the 2 min NO_2 concentration at the top of the hoof, shown in figure 7. Both cases display approximately 2 log reductions corresponding to about the same NO_2 concentration (~2–3 μM), supporting the hypothesis that bacterial inactivation is strongly dependent on NO_2 exposure time and concentration. Furthermore, the bacterial inactivation at the bottom of the hoof displays approximately the same 10 min 'induction time' as the model NO_2 concentration. This correlation supports the hypothesis that antibacterial effects are due to NO_2 diffusing through the nail membrane.

It should be noted that the apparent 'premature' inactivation at 5 and 10 min is within experimental error of 0. It is also

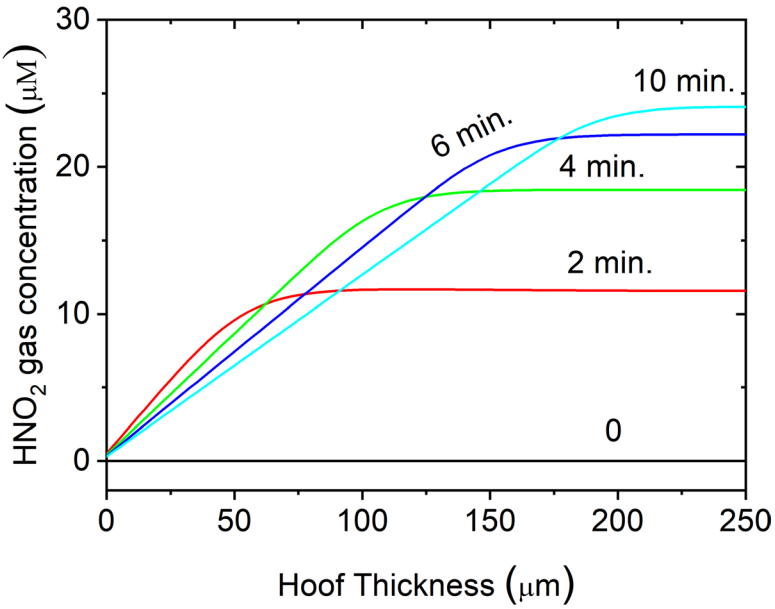

Figure 9. Plot of gas phase HNO_2 as a function of time and position within the membrane, given the assumptions discussed in the text. Uptake and hydrolysis of NO_2 produces both HNO_2 and HNO_3. The latter compound remains on the surface of the keratin fibers, whereas HNO_2 can desorb into the gas phase and diffuse through the hoof membrane. If HNO_2 is allowed to diffuse back out through the top of the hoof but is confined by the pelleted *E. coli* at the bottom of the hoof, it is predicted reach concentrations of over 20 μM within the first 10 min. This could explain the weak but nonzero inactivation shown in figure 8 prior to NO_2 penetration.

possible that a small amount of 'premature' inactivation could actually occur due to the fact that, as seen in reaction (R3), uptake and hydrolysis of NO_2 produces gas phase HNO_2 as well as HNO_3. While HNO_3 does not leave the surface of the keratin fibers, HNO_2 can desorb into the gas phase given its known vapor pressure. Thus, one version of the model was expanded to include HNO_2 desorption from the surface following NO_2 adsorption and hydrolysis followed by gas phase diffusion. This analysis assumed HNO_2 reaching the top of the hoof diffused away and HNO_2 reaching the bottom of the hoof was confined by layers of *E. coli*. As shown in figure 9, HNO_2 is predicted to reach concentrations higher than 20 μM at the far side of the hoof over 10 min given these assumptions. This effect may be responsible for the relatively weak antibacterial effect seen before full penetration of NO_2. However, further studies should be done to better understand this potential mechanism.

4. Conclusions

Many applications of plasma medicine, such as through-nail plasma treatment are dependent on transport of plasma-produced species through a membrane of biological tissue. In this work, we proposed a transient reaction-diffusion model for transport of plasma-generated RNS species through a bovine hoof slice, which serves as a porous biological membrane and a model for a human nail. In the present model, we took NO_2 as the model RNS responsible for most of the observed antimicrobial effects, although it is likely that other species are involved as well. It was shown that physical diffusion alone could not account for the observed time dependence of hoof penetration by NO_2. Rather, transport through the hoof membrane was inhibited by uptake and hydrolysis of NO_2 by water adsorbed on the surface of keratin fibers; only after active surface sites of water were depleted could NO_2 penetrate the hoof membrane. When the fraction of adsorbed water available for NO_2 uptake was set to 10^{-3}, experimental penetration of the hoof membrane agreed well with theoretical results; this suggests that, while NO_2 uptake into the nail is significant, most adsorbed water is strongly bound and cannot take part in uptake.

Comparison to experiments also shows that the uptake-dependent transport of NO_2 through the hoof membrane corresponds to inactivation of *E. coli* on the far side of the hoof. Thus, this model potentially captures the mechanisms responsible for through-nail plasma treatment, observed in a previous report [11]. After an 'induction time' corresponding to the uptake of NO_2 and deactivation of surface sites, NO_2 is predicted to freely diffuse through the hoof membrane and take part in antibacterial (or, depending on the application, antifungal) activity. The thickness of the nail determines not only the steady-state NO_2 penetration rate but also the time needed for diffusing NO_2 to penetrate the membrane. Only minimal bacterial inactivation was observed during the apparent induction time. The observed nonzero inactivation during the induction period is provisionally attributed to the diffusion of HNO_2 formed by hydrolysis of NO_2 within the nail. This effect is relatively weak in comparison to the inactivation that takes place after the induction time is over and NO_2 fully penetrates the nail.

This work provides a theoretical and quantitative model of the mechanisms of through-nail plasma treatment, which is relevant to applications such as plasma treatment of onychomycosis. The importance of NO_2 uptake by adsorbed water is shown, and a correlation is observed between bacterial inactivation and the reaction-diffusion mechanisms presented

in this paper. While this study used a biological membrane, the findings are relevant in a broader context as well, since adsorbed water will commonly be present on membranes in atmospheric air. Thus, the findings of this paper potentially provide basic insights into other plasma treatments through porous membranes at atmospheric pressure.

Acknowledgments

The authors gratefully acknowledge partial support from Department of Energy OFES Grant No. DE-SC0001939, National Science Foundation Grant No. 1606062, and the Korean Institute of Energy Technology Evaluation and Planning (KETEP) grant funded by the Korean Government Ministry of Trade, Industry and Energy (20172010104830).

ORCID iDs

Daniel T Elg https://orcid.org/0000-0001-7130-3613

References

[1] Graves D B 2012 The emerging role of reactive oxygen and nitrogen species in redox biology and some implications for plasma applications to medicine and biology *J. Phys. D: Appl. Phys.* **45** 263001
[2] Kong M G, Kroesen G, Morfill G, Nosenko T, Shimizu T, van Dijk J and Zimmermann J L 2009 Plasma medicine: an introductory review *New J. Phys.* **11** 115012
[3] Fridman G, Friedman G, Gutsol A, Shekhter A B, Vasilets V N and Fridman A 2008 Applied plasma medicine *Plasma Process. Polym.* **5** 503–33
[4] Stoffels E, Sakiyama Y and Graves D B 2008 Cold atmospheric plasma: charged species and their interactions with cells and tissues *IEEE Trans. Plasma Sci.* **36** 1441–57
[5] Laroussi M 2005 Low temperature plasma-based sterilization: overview and state-of-the-art *Plasma Process. Polym.* **2** 391–400
[6] Lloyd G, Friedman G, Jafri S, Schultz G, Fridman A and Harding K 2010 Gas plasma: medical uses and developments in wound care *Plasma Process. Polym.* **7** 194–211
[7] Sakiyama Y, Graves D B, Chang H-W, Shimizu T and Morfill G E 2012 Plasma chemistry model of surface microdischarge in humid air and dynamics of reactive neutral species *J. Phys. D: Appl. Phys.* **45** 425201
[8] Orazov M, Sakiyama Y and Graves D B 2012 Wound healing modeling: investigating ambient gas plasma treatment efficacy *J. Phys. D: Appl. Phys.* **45** 445201
[9] Stalder K R, McMillen D F and Woloszko J 2005 Electrosurgical plasmas *J. Phys. D: Appl. Phys.* **38** 1728–38
[10] von Woedtke T, Reuter S, Masur K and Weltmann K D 2013 Plasmas for medicine *Phys. Rep.* **530** 291–320
[11] Xiong Z L, Roe J, Grammer T C and Graves D B 2016 Plasma treatment of onychomycosis *Plasma Process. Polym.* **13** 588–97
[12] Pavlovich M J, Clark D S and Graves D B 2014 Quantification of air plasma chemistry for surface disinfection *Plasma Sources Sci. Technol.* **23** 065306
[13] Monti D, Saccomani L, Chetoni P, Burgalassi S, Tampucci S and Mailland F 2011 Validation of bovine hoof slices as a model for infected human toenails: *in vitro* ciclopirox transungual permeation *Br. J. Dermatol.* **165** 99–105
[14] Nogueiras-Nieto L, Gomez-Amoza J L, Delgado-Charro M B and Otero-Espinar F J 2011 Hydration and N-acetyl-l-cysteine alter the microstructure of human nail and bovine hoof: implications for drug delivery *J. Control. Release* **156** 337–44
[15] Pavlovich M J, Chang H W, Sakiyama Y, Clark D S and Graves D B 2013 Ozone correlates with antibacterial effects from indirect air dielectric barrier discharge treatment of water *J. Phys. D: Appl. Phys.* **46** 145202
[16] Wood B D, Quintard M and Whitaker S 2002 Calculation of effective diffusivities for biofilms and tissues *Biotechnol. Bioeng.* **77** 495–516
[17] Vaupel P 1976 Effect of percentual water-content in tissues and liquids on diffusion-coefficients of O_2, CO_2, N_2, and H_2 *Pflug. Arch. Eur. J. Phys.* **361** 201–4
[18] Ho Q T, Verlinden B E, Verboven P, Vandewalle S and Nicolai B M 2006 A permeation–diffusion–reaction model of gas transport in cellular tissue of plant materials *J. Exp. Bot.* **57** 4215–24
[19] King G 1945 Permeability of keratin membranes to water vapour *Trans. Faraday Soc.* **41** 479–87
[20] Skinn B T and Deen W M 2013 A nitrogen dioxide delivery system for biological media *Free Radic. Biol. Med.* **56** 44–53
[21] Gunt H B and Kasting G B 2007 Equilibrium water sorption characteristics of the human nail *J. Cosmet. Sci.* **58** 1–9
[22] Shiraiwa M, Sosedova Y, Rouviere A, Yang H, Zhang Y, Abbatt J P, Ammann M and Poschl U 2011 The role of long-lived reactive oxygen intermediates in the reaction of ozone with aerosol particles *Nat. Chem.* **3** 291–5
[23] Kleffmann J, Becker K H, Lackhoff M and Wiesen P 1999 Heterogeneous conversion of NO_2 on carbonaceous surfaces *Phys. Chem. Chem. Phys.* **1** 5443–50
[24] Aumont B, Madronich S, Ammann M, Kalberer M, Baltensperger U, Hauglustaine D and Brocheton F 1999 On the NO_2 plus soot reaction in the atmosphere *J. Geophys. Res.-Atmos.* **104** 1729–36
[25] Squadrito G L and Postlethwait E M 2009 On the hydrophobicity of nitrogen dioxide: could there be a 'lens' effect for NO_2 reaction kinetics? *Nitric Oxide* **21** 104–9
[26] Choi W and Leu M T 1998 Nitric acid uptake and decomposition on black carbon (soot) surfaces: its implications for the upper troposphere and lower stratosphere *J. Phys. Chem.* A **102** 7618–30
[27] Jenkin M E, Cox R A and Williams D J 1988 Laboratory studies of the kinetics of formation of nitrous-acid from the thermal-reaction of nitrogen-dioxide and water-vapor *Atmos. Environ.* **22** 487–98
[28] Goodman A L, Underwood G M and Grassian V H 1999 Heterogeneous reaction of NO_2: characterization of gas-phase and adsorbed products from the reaction, $2NO_2(g) + H_2O(a) \rightarrow HONO(g) + HNO_3(a)$ on hydrated silica particles *J. Phys. Chem.* A **103** 7217–23
[29] Seisel S, Börensen C, Vogt R and Zellner R 2005 Kinetics and mechanism of the uptake of N_2O_5 on mineral dust at 298 K *Atmos. Chem. Phys.* **5** 3423–32
[30] Mertes S and Wahner A 1995 Uptake of nitrogen-dioxide and nitrous-acid on aqueous surfaces *J. Phys. Chem.* **99** 14000–6
[31] Acker K B D and Moller D 2008 Nitrite in dew, fog, cloud and rain water: an indicator for heterogeneous processes on surfaces *Atomos. Res.* **87** 200–12
[32] Murdachaew G, Varner M E, Phillips L F, Finlayson-Pitts B J and Gerber R B 2013 Nitrogen dioxide at the air–water interface: trapping, absorption, and solvation in the bulk and at the surface *Phys. Chem. Chem. Phys.* **15** 204–12
[33] Grätzel M, Henglein A, Lilie J and Beck G 1969 Pulsradiolytische Untersuchung einiger Elementarprozesse der Oxydation und Reduktion des Nitritions *Berich. Bunsen. Gesell.* **73** 631–730

[34] Saastad O W, Ellermann T and Nielsen C J 1993 On the adsorption of NO and NO_2 on cold H_2O/H_2SO_4 surfaces *Geophys. Res. Lett.* **20** 1191–3
[35] Komiyama H and Inoue H 1980 Absorption of nitrogen oxides into water *Chem. Eng. Sci.* **35** 154–61
[36] Leider M and Buncke C M 1954 Physical dimensions of the skin—determination of the specific gravity of skin, hair, and nail *Ama. Arch. Derm. Syph.* **69** 563–9
[37] Schwartz S E and White W H 1981 Solubility equilibria of the nitrogen oxides and oxyacids in dilute aqueous solution *Adv. Environ. Sci. Eng.* **4** 1–46
[38] Miller Y, Finlayson-Pitts B J and Gerber R B 2009 Ionization of N_2O_4 in contact with water: mechanism, time scales and atmospheric implications *J. Am. Chem. Soc.* **131** 12180–5
[39] Ammann M, Poschl U and Rudich Y 2003 Effects of reversible adsorption and Langmuir–Hinshelwood surface reactions on gas uptake by atmospheric particles *Phys. Chem. Chem. Phys.* **5** 351–6
[40] Medeiros D D and Pimentel A S 2011 New insights in the atmospheric HONO formation: new pathways for N_2O_4 isomerization and NO_2 dimerization in the presence of water *J. Phys. Chem.* A **115** 6357–65